Model of reentrant ventricular tachycardia based on infarct border zone geometry predicts reentrant circuit features as determined by activation mapping

Edward J. Ciaccio, PhD,*† Hiroshi Ashikaga, MD, PhD,§ Riyaz A. Kaba, MD,‖ Daniel Cervantes, MD,* Bruce Hopenfeld, PhD,§ Andrew L. Wit, PhD,* Nicholas S. Peters, MD, PhD,‖ Elliot R. McVeigh, PhD,§ Hasan Garan, MD,‡ James Coromilas, MD‡

*From the Departments of *Pharmacology, †Biomedical Engineering, and ‡Medicine, Columbia University, New York, New York, §Laboratory of Cardiac Energetics, The National Heart, Lung and Blood Institute, Bethesda, Maryland, and ‖Department of Medicine, St. Mary's Hospital, Imperial College London, London, United Kingdom.*

BACKGROUND Infarct border zone (IBZ) geometry likely affects inducibility and characteristics of postinfarction reentrant ventricular tachycardia, but the connection has not been established.

OBJECTIVE The purpose of this study was to determine characteristics of postinfarction ventricular tachycardia in the IBZ.

METHODS A geometric model describing the relationship between IBZ geometry and wavefront propagation in reentrant circuits was developed. Based on the formulation, slow conduction and block were expected to coincide with areas where IBZ thickness (T) is minimal and the local spatial gradient in thickness (ΔT) is maximal, so that the degree of wavefront curvature $\rho \propto \Delta T/T$ is maximal. Regions of fastest conduction velocity were predicted to coincide with areas of minimum ΔT. In seven arrhythmogenic postinfarction canine heart experiments, tachycardia was induced by programmed stimulation, and activation maps were constructed from multichannel recordings. IBZ thickness was measured in excised hearts from histologic analysis or magnetic resonance imaging. Reentrant circuit properties were predicted from IBZ geometry and compared with ventricular activation maps after tachycardia induction.

RESULTS Mean IBZ thickness was 231 $\pm$ 140 μm at the reentry isthmus and 1440 $\pm$ 770 μm in the outer pathway ($P < 0.001$). Mean curvature ρ was 1.63 $\pm$ 0.45 mm^{-1} at functional block line locations, 0.71 $\pm$ 0.18 mm^{-1} at isthmus entrance-exit points, and 0.33 $\pm$ 0.13 mm^{-1} in the outer reentrant circuit pathway. The mean conduction velocity about the circuit during reentrant tachycardia was 0.32 $\pm$ 0.04 mm/ms at entrance-exit points, 0.42 $\pm$ 0.13 mm/ms for the entire outer pathway, and 0.64 $\pm$ 0.16 mm/ms at outer pathway regions with minimum ΔT. Model sensitivity and specificity to detect isthmus location was 75.0% and 97.2%.

CONCLUSIONS Reentrant circuit features as determined by activation mapping can be predicted on the basis of IBZ geometrical relationships.

KEYWORDS Arrhythmia; Border zone; Conduction velocity; Infarction; Mapping; MRI; Propagation; Ventricular tachycardia

(Heart Rhythm 2007;4:1034–1045)

Introduction

Postinfarction reentrant ventricular tachycardia is an important clinical problem, yet locating the circuit can be problematic.[1,2] Electrical activation mapping is currently used for pinpointing reentrant circuit location, but the procedure is often time-consuming and is limited by the fact that clinical tachycardia cannot always be induced during electrophysiological study and/or it may not be well tolerated hemodynamically. As cardiac magnetic resonance technology improves,[3] attention has recently been focused on the possibility that the structural characteristics of the infarct and the infarct border zone (IBZ) may be correlated to the characteristics of the circuit causing postinfarction reentrant ventricular tachycardia. In canine postinfarction hearts, the reentrant circuit isthmus has been shown to overlap the thinnest IBZ, and functional block lines tend to coincide with sharper transitions to thicker tissue about the isthmus.[4,5] Both the isthmus and the functional block lines tend to remain approximately constant in location during any particular reentrant circuit morphology.[6,7] When multiple reentrant circuit morphologies are inducible in the canine IBZ, we have observed that the isthmus location of most or all of the morphologies coincide, with a difference in isthmus

This study was supported by an Established Investigator Award no. 9940237N from the American Heart Association and a Whitaker Foundation Research Award (to EJC), National Institutes of Health-National Heart, Lung and Blood Institute (NIH-NHLBI) Intramural grant no. Z01-HL4004609 (to ERM), NIH-NHLBI Program Project grant no. HL30557 (to ALW), and British Heart Foundation grant no. RG/05/009 (to NSP). **Address reprint requests and correspondence:** Edward J. Ciaccio, Ph.D., PH7W-Pharmacology, Columbia University, 630 West 168th Street, New York, NY 10032. E-mail address: ejc6@columbia.edu. (Received March 2, 2007; accepted April 7, 2007.)

1547-5271/$ -see front matter doi:10.1016/j.hrthm.2007.04.015

entrance and exit points being the distinguishing characteristic.[6–8] These observations suggest that there is a relationship between structure and electrical conduction in the IBZ during tachycardia.

If a geometric model relating IBZ structure to reentry conduction characteristics could be developed, it would then be possible to predict the reentrant circuit pattern and characteristics from imaging data of the infarct and border zone (BZ). Since cardiac magnetic resonance technology is becoming sufficiently sophisticated to image these areas of the heart at high resolution,[3,9,10] it is possibile to use the geometric formulation to pinpoint the isthmus and candidate ablation sites in postinfarction patients with recurrent ventricular tachycardia. In this study, we describe the development of a geometric model to show the relationship between IBZ structure and wavefront propagation in canine postinfarction reentrant tachycardia and use it to predict reentry isthmus location and candidate ablation sites. The formulation is based on the fact that geometric changes in the conducting medium give rise to changes in wavefront curvature. We hypothesized that wavefront curvature and the resulting impedance mismatch, as caused by sharp IBZ thickness transitions at the isthmus lateral edges, would be sufficient to form functional block lines about which the reentrant circuit would propagate. We hypothesized that wavefront curvature caused by lesser IBZ thickness changes at the isthmus ends and elsewhere in the path of the circuit would be insufficient to cause functional block at those locations. These hypotheses were tested by calculating the degree of wavefront curvature as estimated by the geometric model at locations of actual functional block, at isthmus entrance and exit points, and elsewhere in the circuit and by determining the degree of overlap of actual versus estimated isthmus location.

Methods

Data collection and measurement

In seven mongrel canines weighing 20–40 kg, the left anterior descending (LAD) coronary artery was ligated near its base under sodium pentobarbital anesthesia (30 mg/kg intravenously).[11] The resulting infarction in the anterior left ventricle (LV) resulted in an IBZ that extended to the epicardium. The animals were prepared for electrophysiologic analysis 3–5 days after LAD ligation, and programmed electrical stimulation was used to induce tachycardia. Electrograms from the epicardial surface of the IBZ were recorded using a multichannel bipolar array and data acquisition system, and activation maps of sinus rhythm and ventricular tachycardia were then constructed. From reentrant ventricular tachycardia maps, the isthmus border was defined as the location of bounding functional lines of block that were connected by straight lines at their ends.[12,13] The outer pathway was defined as the reentrant circuit location outside the isthmus where it still overlapped the infarct. After electrophysiologic analysis, the heart was excised and prepared for thickness measurement using either histologic analysis (n = 4 canine postinfarction experiments) or magnetic resonance imaging (MRI) analysis (n = 3 experiments). Further details are provided in the online supplement.

Thickness measurement

Thickness measurements (1-μm resolution) were made from histology images using computer software (Spot Diagnostic Instruments, Sterling Heights, MI). An arrow was projected at right angles from the connective tissue layer at the epicardial surface to the necrotic region of infarcted tissue at depth (Figure 1A, 1B). The arrow length (IBZ thickness T) was calculated automatically, and the isthmus region tended to be thinner than the outer pathway (Figure 1A, 1B). The tissue samples for histology thickness measurements were taken at 5-mm intervals over a 5 cm $\times$ 5 cm area of the IBZ (100 total slides). Six thickness measurements were made at random locations on each slide and averaged. An IBZ thickness map was constructed after interpolating and smoothing the XY coordinates to a final resolution of 0.4 mm $\times$ 0.4 mm in the surface plane (Figure 1C). Thickness measurements with 1-μm resolution were made from MRI images using ImageJ (National Institutes of Health, Bethesda, MD). Each MRI slice had a pixel resolution of 0.4 mm $\times$ 0.4 mm, and the distance between slices was 0.4 mm. A representative slice is shown in false color with thickness measurement lines denoted in black (Figure 1E; view is from base to apex). Measurement lines were spaced ~2 mm apart by hand and extended from the connective tissue layer to the contiguous infarct (yellow-white in Figure 1E) or to the concavity of the endocardial surface excluding the papillary muscles (denoted in part by the gray line). The line length (IBZ thickness T) and its position in Cartesian coordinates were automatically computed by ImageJ. From all sample points, a three-dimensional LV thickness map was constructed using map3d[14] (Figure 1D, 1F). The approximate slice location of panel E is denoted by the black dashed lines in panels D and F. Correspondences between the MRI map (panel E) and thickness maps (panels D, F) are shown at selected locations by gray and green circles. The thinnest area in the IBZ is ~50 μm (dark blue, Figure 1D, 1E), and it overlaps the reentry isthmus location (denoted by two bordering black lines that signify areas of functional block during tachycardia). Thickest LV regions are ~9.5 mm (dark red, Figure 1D, 1F).

Geometry-to-propagation model: Relationships that provide a basis for equations

During reentrant ventricular tachycardia, we propose that activation wavefront curvature is related to IBZ geometry as depicted in Figure 2. A diagram of wavefront propagation during the extrastimulation cycle is shown in Figure 2A. The stimulus location is at left, and arrows denote the direction of activation. When stimulating from outside the IBZ, the premature stimulus, depending on the S1-S2 coupling interval, blocks within the BZ near its boundary with the normal zone (NZ) (BZ mean refractory period of ~199 ms; NZ mean refractory period ~159 ms).[15] The wavefront

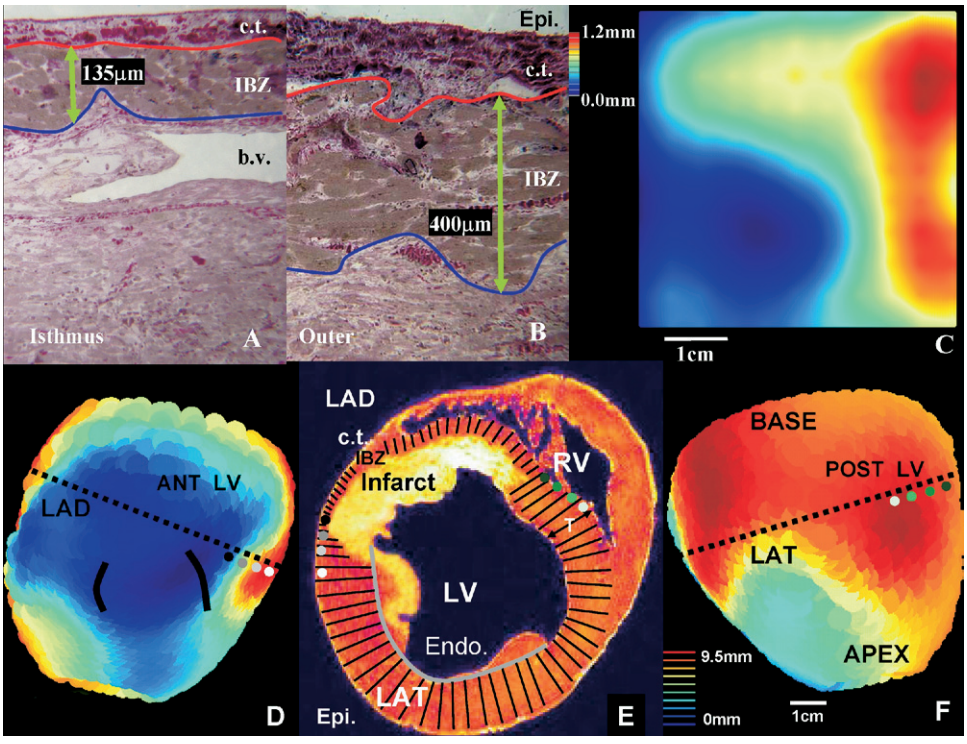

Figure 1 Method to measure IBZ thickness. **A–C:** Histology measurement. Adjacent wax sections were stained with Masson's trichrome stain to distinguish infarcted from surviving myocytes. **D–F:** MRI measurement. **E:** The ex-vivo MR scanning provides a view of the heart slice from above (base to apex).

then bifurcates and gradually activates the entire IBZ including the region where the isthmus will form, turning in the opposite direction and eventually breaking through the unidirectional block line to initiate reentry. In Figure 2B, three-dimensional wavefront curvature is depicted during a reentry cycle. The infarct is shown in green, and the epi-

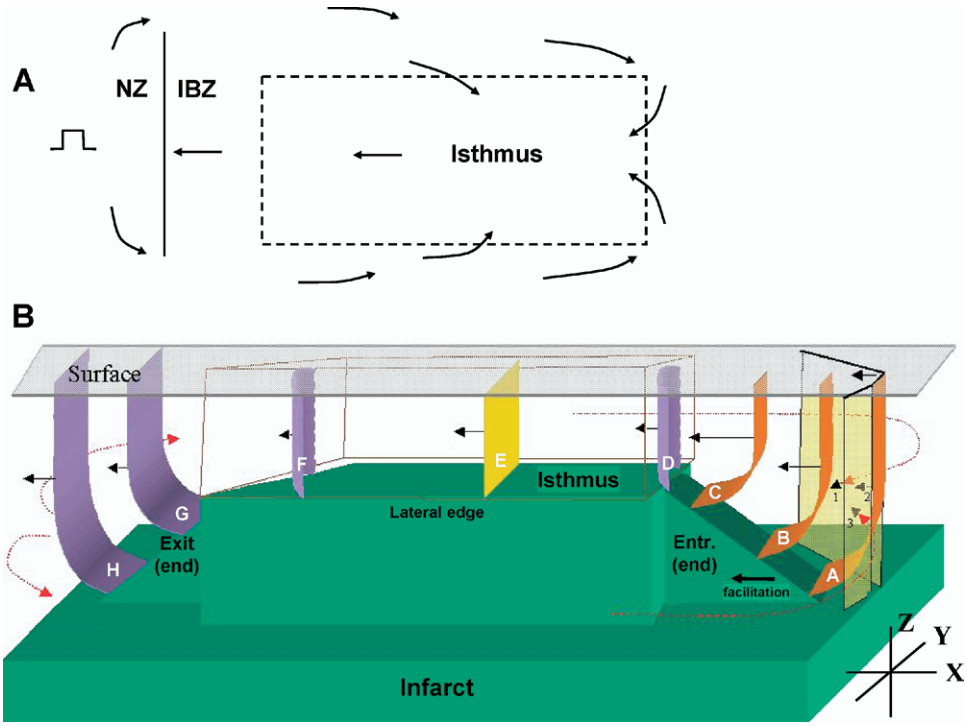

Figure 2 Characteristics of reentrant ventricular tachycardia. **A:** Diagram of the extrastimulation cycle leading to reentry. **B:** Schematic of the proposed relationship between IBZ thickness (*Z*-axis) and wavefront curvature when propagation within the reentrant circuit is parallel to the plane of the epicardial surface (*XY*).

cardial surface is shown as a clear sheet at the top. As described in previous studies by our group,[4,5] a rectangular plateau of the thinnest IBZ coincides with the reentry isthmus. At the plateau's lateral boundaries, step changes in infarct depth correspond with functional block line locations, whereas at the plateau's ends, gradual thickness changes (ramps) coincide with entrance and exit points to the isthmus. The expected three-dimensional wavefront curvature at various locations during reentry is denoted by surfaces that are concave (orange), rectilinear or flat (yellow), or convex (violet), and propagation direction during a reentry cycle is denoted by arrows.

Near the isthmus entrance, the wavefront is concave[16–18] in the *XY*-plane because of convergence of the two bifurcated portions of the double-loop wavefront (denoted as transparent sheets labeled 1–3). Concave curvature also occurs along the thickness axis (*Z*-axis) due to diminishing IBZ thickness during propagation toward the plateau (wavefronts A–C). Since concave curvature causes the wavefront to accelerate,[16–18] conduction is facilitated toward the isthmus perimeter, which is therefore the fastest direction for propagation. At the isthmus entrance, the wavefront proceeds through a narrowed aperture where it is constrained by the bounding functional arcs of block, and then it suddenly becomes convex in the *XY*-plane at the distal expansion into the isthmus (point D). Since convex curvature causes the wavefront to decelerate, propagation is slowed at point D and there is the potential for block. The wavefront does not block at this expansion as long as the safety factor remains above unity, which is in part facilitated by the extra current available within one space constant before the aperture.[18,19] Hence, entrance to the isthmus is more likely to succeed when wavefront curvature is concave toward the entrance point and the incidence angle is 90°, which will occur when there is a gradual decrease in IBZ thickness in that direction, as shown.

Within the isthmus, if infarct depth and the distance to the lateral walls in the *XY*-plane is level, then the wavefront becomes flat (E). At the isthmus exit, the wavefront becomes convex along the *XY*-plane at the distal expansion away from the block lines (F) and along the *Z*-axis due to increasing IBZ thickness after the exit point (G and H). When thickness increases more gradually away from the exit, *Z*-axis convexity is reduced, increasing the safety factor so that the wavefront is more likely to propagate. Hence, successful propagation out of the isthmus would be expected to occur at an edge of the plateau having a relatively gradual thickness increase in the radially outward direction (as at the actual exit point in Figure 2B). About the lateral isthmus edges where there is a step change in thickness, functional block would be expected to occur because of the large wavefront convexity along the *Z*-axis as it propagates radially outward at those locations. In the case of approximately symmetric geometry about the isthmus (Figure 2B), either end can potentially act as an entrance or exit depending on the extrastimulation point, that is, two opposite reentrant circuit morphologies would be possible, as has actually been observed in other canine postinfarction experiments.[6–8]

Geometry to propagation: Model equations

Based on the above description, we sought to develop a set of equations relating IBZ geometry to excitation wavefront propagation. The velocity of impulse conduction without curvature θ_o is dependent on the longitudinal resistance R of the conducting medium[18]:

$$\theta_o^2 \propto 1/R \tag{1}$$

The overall conduction velocity is

$$\theta = \theta_o + \theta_c, \tag{2}$$

where the conduction velocity contribution θ_c is due to wavefront curvature. In the BZ, θ_c can be estimated as follows:

$$\theta_c = D\rho, \tag{3}$$

where D is the diffusion coefficient (the current flow due to the transmembrane potential gradient, with a value of $0.05 - 0.2$ mm^2/ms in ventricular myocardium[20]) and ρ is the degree of wavefront curvature in units of mm^{-1}. Thus,

$$\theta = \theta_o + D\rho, \tag{4a}$$

$$= \theta_o - D/r, \tag{4b}$$

where r is the local radius of curvature.

As a first approximation, suppose that no-flux conditions exist at lateral borders,[16,21] so that the wavefront edges must be perpendicular to the boundary points. When propagating through constrained regions with no-flux boundaries, wavefront curvature can be modeled as a circular arc.[16] As depicted in Figure 3A,

$$r = (w/2)/\sin(\beta) \tag{5}$$

where r is the radius of the circle forming the wavefront shape, w is the chord width, and β is the angle from the midline to the lateral borders. For canine postinfarction, the IBZ is bounded along the Z-axis (thickness axis) by the infarct at depth and by the epicardial surface of the heart. If the wavefront propagates in parallel with the surface, then β is a constant 0° in that direction but will vary in the infarct direction. Figure 3B shows the geometric principles. Suppose the activation wavefront is propagating up an incline (spatial decrease in IBZ thickness) toward the isthmus entrance as from point i to $i + 1$. IBZ thickness changes from T_i to T_{i+1} as shown. The change in thickness is ΔT_i, the space step from i to $i + 1$ is a distance c, the angle with the infarct surface in the direction of propagation is β_1, and the angle with the heart surface in the direction of propagation is $\beta_2 = 0°$. At each space step, curvature in the *XZ*-plane is calculated. From trigonometry we can estimate

$$\sin(\beta) = \Delta T/(c^2 + \Delta T^2)^{1/2}. \tag{6}$$

Substituting Equations 5 and 6 into Equation 4b,

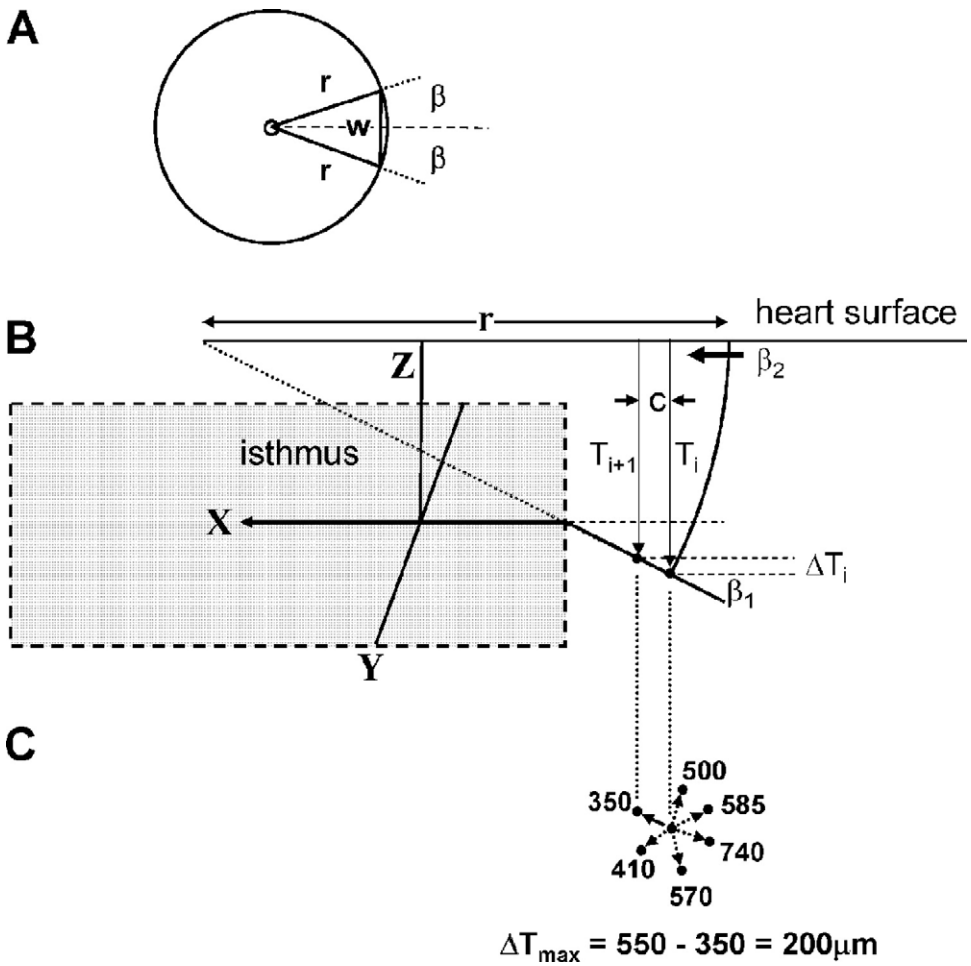

Figure 3 Mathematical relationships used to formulate the geometric model. **A:** Wavefront curvature as a circular arc. **B:** Geometrical configuration for calculating wavefront curvature due to IBZ thickness change. **C:** Method to determine the maximum thickness change (ΔT_{max}) in proximity to a particular computational node.

$$\theta = \theta_o - D \cdot \Delta T/[T \cdot (c^2 + \Delta T^2)^{1/2}], \quad (7)$$

where $w/2 = T$ (Figure 3A, 3B). Thus

$$\rho = -\Delta T/[T \cdot (c^2 + \Delta T^2)^{1/2}]. \quad (8)$$

Let ΔT_{max} at a particular node (x, y) be the largest absolute magnitude change in thickness in the vector field about a local region in any direction $(x + \Delta x, y + \Delta y)$. In Figure 3C, hypothetical thickness values in microns are shown surrounding node i. Let $T_i = 550$ μm. The surrounding thickness values with greatest difference from T_i, 350 and 740 μm, are oriented approximately in the direction of greatest incline in Figure 3B. Based on these hypothetical values at node i, $\Delta T_{max} = 550$ μm $- 350$ μm $= 200$ μm. From the ΔT_{max} calculated at any particular node, the maximum possible degree of wavefront curvature in the vector field about that node is

$$\rho_{max} = \Delta T_{max}(x, y)/[T(x, y) \cdot (c^2 + \Delta T_{max}(x, y)^2)^{1/2}], \quad (9)$$

which occurs when the wavefront propagates across the node in the direction of largest ΔT. At any IBZ areas where the spatial change in thickness is relatively small $(\Delta T_{max} << c)$,

$$\rho_{max} \approx \Delta T_{max}/(c \cdot T). \quad (10)$$

In ventricular myocardium, it has been shown experimentally and by computer model[17,22] that block occurs at a typical ventricular tachycardia cycle length in canine postinfarction (175–225 ms) when $r \sim 1$ mm. Therefore, we would anticipate that an absolute value of $\rho_{max} \geq\approx 1$ mm^{-1}, as estimated by Equations 9 and 10, would be indicative of very slow conduction or block during reentrant tachycardia when the wavefront propagates from the thinner isthmus region radially outward to areas of thicker viable tissue (convex wavefront curvature).

To predict regions with most rapid conduction velocity in the IBZ during reentrant tachycardia, suppose that the total change in thickness Z from isthmus to outer pathway or vice versa occurs at a single space step j:

$$dT_i = Z, i = j,$$

$$dT_i = 0, i \neq j.$$

In the direction from thinner to thicker tissue (isthmus to outer pathway), very slow conduction or block will occur at j if Z is sufficiently large because of the large convex wavefront curvature at the step change in tissue thickness (large impedance mismatch). In the direction from thicker to thinner tissue (outer pathway to isthmus), a transient increase in θ will occur at space step j because of the concave wavefront curvature, but $\theta = \theta_o$ elsewhere along the path. We can postulate that in either direction, gradual rather than step changes in T will minimize the transit time (TT) over n space steps. TT can be estimated by substituting Equation 10, which is useful when ΔT is of low magnitude along the path of propagation, into Equation 4a, with ρ estimated as ρ_{max}, and then inverting and writing as a differential

$$\begin{aligned} TT &= \sum\{1/[\theta_o - (DdT_i)/(c \cdot T_i)]\}, \\ &= \sum\{T_i/[\theta_o T_i - (D/c)\, dT_i]\}, \end{aligned} \tag{11}$$

for $i = 1$ to n space steps. Since $T_{i+1} = T_i + dT_i$ and dT_i is the thickness change between space steps i and $i + 1$,

$$\begin{aligned} TT &= \sum\{T_i/[\theta_o T_i - (D/c)T_{i+1} + (D/c)T_i]\} \\ &= \sum\{T_i/[(\theta_o + D/c)T_i - (D/c)T_{i+1}]\}. \end{aligned} \tag{12}$$

Let $c_1 = \theta_o + D/c$, $c_2 = D/c$, and v represent the denominator. To minimize TT from thin tissue (isthmus location) to thick tissue (outer pathway) or vice versa, the quotient rule is used and the equation set to zero:

$$\begin{aligned} 0 &= \sum\{[c_1 T_i dT_i - c_2 T_i dT_{i+1}] - [c_1 T_i dT_i - c_2 T_{i+1} dT_i]\}/v^2 \\ 0 &= \sum\{c_2(T_i\, dT_{i+1} - T_{i+1}\, dT_i)\}/v^2. \end{aligned} \tag{13}$$

Thus

$$\sum (T_i\, dT_{i+1})/v^2 = \sum (T_{i+1}\, dT_i)/v^2, \tag{14}$$

which has an approximate solution of

$$dT_i = dT_{i+1} = Z/n,\ i = 0, \text{to } n-1 \tag{15}$$

for n space steps and a total thickness change Z from isthmus to outer pathway or vice versa, regardless of whether the sign of dT_i is positive or negative (wavefront convex or concave). Thus, according to Equation 15, a constant, minimized thickness change ΔT along the path would be expected to minimize TT and therefore maximize θ whether traveling from the isthmus to outer pathway or vice versa.

Measurements and statistics

We computed ΔT_{max} (see Figure 3C) from $N = 25$ surrounding points to calculate, from Equation 9, ρ_{max} at all grid nodes. From maps of these values, estimated block lines were drawn in the center of distinct regions having $\rho_{max} > 1\ mm^{-1}$. The estimated line locations were compared with actual block line locations determined from tachycardia activation mapping by averaging the distances between five equally spaced corresponding points on each line. We drew a straight line between the midpoints of the estimated block lines on the grid and calculated the percentage of actual isthmus width that would be blocked if this line was used as an estimated ablation line. Areas of fastest conduction velocity about the reentrant circuit were estimated, according to the result given in Equation 15, to be contiguous regions with minimum ΔT_{max}. We selected a threshold $\Delta T_{max} < 0.05$ mm/mm, that is, <25% of the largest expected ΔT_{max} of ~0.2 mm/mm in close proximity to the isthmus that was observed previously.[5] Actual reentrant ventricular tachycardia conduction velocity was measured at five random points on the activation map in the region with minimum ΔT_{max}, at five random points at entrance-exit areas, and from five random points throughout the outer pathway and averaged over each of these three regions. Conduction velocity was measured as the distance between a pair of adjacent recording sites divided by the difference in activation time between them. The sites were selected such that the vector orientation overlapping their locations was parallel to the direction of wavefront propagation.

The unpaired t-test and one-way analysis of variance were used to determine the statistical significance of the difference in means between variables ($P < .05$). The sensitivity of the geometric model for detecting isthmus location was calculated as the area of the actual isthmus that was overlapped by the estimated isthmus divided by the area of the actual isthmus. The specificity was calculated as the area of the BZ that was not overlapped by the actual or estimated isthmus divided by the area of the BZ that was not overlapped by the actual isthmus. Because we did not measure the entire extent of the IBZ in histology experiments, we used a constant 5 cm × 5 cm area as the approximate area of the BZ for all specificity calculations. Measurements of area (actual area from activation and estimated area from ρ_{max}) and their overlap were determined from the computerized maps using ImageJ.

Results

Of seven canine postinfarction experiments, four had only inducible sustained reentrant ventricular tachycardia with a mappable circuit (single morphologies), two had only inducible nonsustained reentrant ventricular tachycardia with a mappable circuit (single morphologies), and one had inducible tachycardia but no mappable reentrant circuit.

An example of activation mapping and analysis of infarct depth after histologic measurement is given in Figure 4. The panels show activation maps of sinus rhythm (Figure 4A), tachycardia (Figure 4B), thickness map T (Figure 4C), maximum gradient ΔT_{max} (Figure 4D), maximum curvature ρ_{max} estimated from Equation 9 (Figure 4E), and the bipolar electrode grid configuration (Figure 4F). Colors from red to blue denote early-to-late activation with isochrones spaced 10–20 ms apart (Figure 4A, 4B), larger to smaller thickness T (Figure 4C), and greater to lesser ΔT_{max} and ρ_{max} (Figure 4D, 4E). In the tachycardia activation map (Figure 4B), conduction block is denoted by thick curved black lines, the wavefront propagation direction is given by arrows, and the thickness measurement area is delineated by the square. Tachycardia is caused by a double-loop reentrant circuit

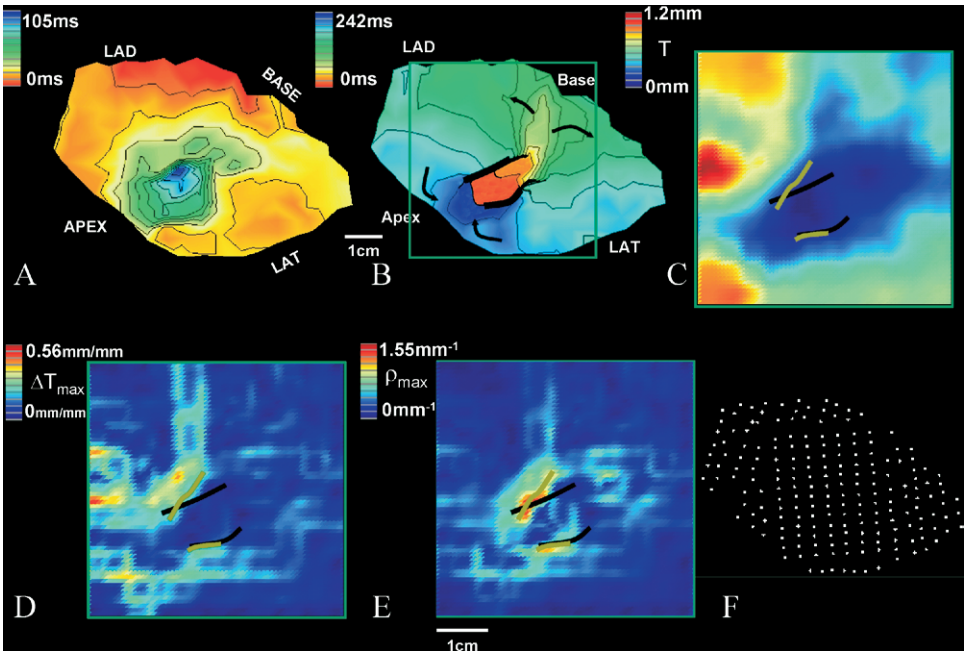

Figure 4 IBZ maps for a selected postinfarction canine experiment. **A and B:** Activation during sinus rhythm and ventricular tachycardia. Thin lines separating colors denote isochrones. **C:** IBZ thickness T determined from histology slides. **D:** Thickness gradient ΔT_{max}. **E:** The value of ρ_{max} estimated from Equation 9. Overlaid are the locations of estimated (*gray-green*) and actual (*black*) lines of block (also in Figures 5–7). **F:** The multielectrode grid.

(Figure 4B, arrows) with slow sinus rhythm activation at the isthmus region (Figure 4A). The IBZ is thinnest at the approximate isthmus location (Figure 4C), and relatively steep thickness changes ΔT_{max} occur near the lateral boundaries (Figure 4D). Estimated functional block line locations were derived from the map of Figure 4E and are centered at areas of greatest ρ_{max} (gray-green lines); actual block line locations are overlaid on the map (black lines). Actual and estimated line locations were then also overlapped on panels C and D. The estimated and actual arcs of block do not precisely coincide (also in Figure 5), which is likely due in part to slight measurement error and distortion during the projection process. Not all areas of large ΔT_{max} (Figure 4D) are manifested as areas with large ρ_{max} (Figure 4E) because

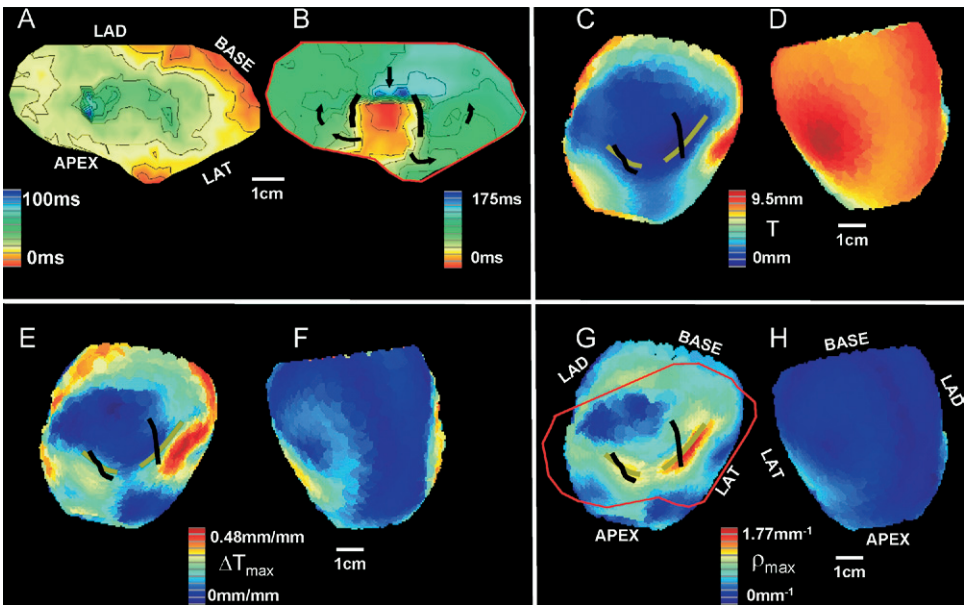

Figure 5 IBZ maps for a postinfarction canine experiment in which sustained reentrant tachycardia was inducible by extrastimulation. **A and B:** Activation during sinus rhythm and ventricular tachycardia. **C and D:** IBZ thickness T determined from MRIs. **E and F:** Thickness gradient ΔT_{max}. **G and H:** Maximum degree of curvature ρ_{max} estimated from Equation 9. Estimated block lines computed from panel **G** (*gray*), and actual block lines determined from the ventricular tachycardia activation map in panel **B** (*black*) are overlaid on the maps in panels **C, E**, and **G** (also in Figures 6 and 7).

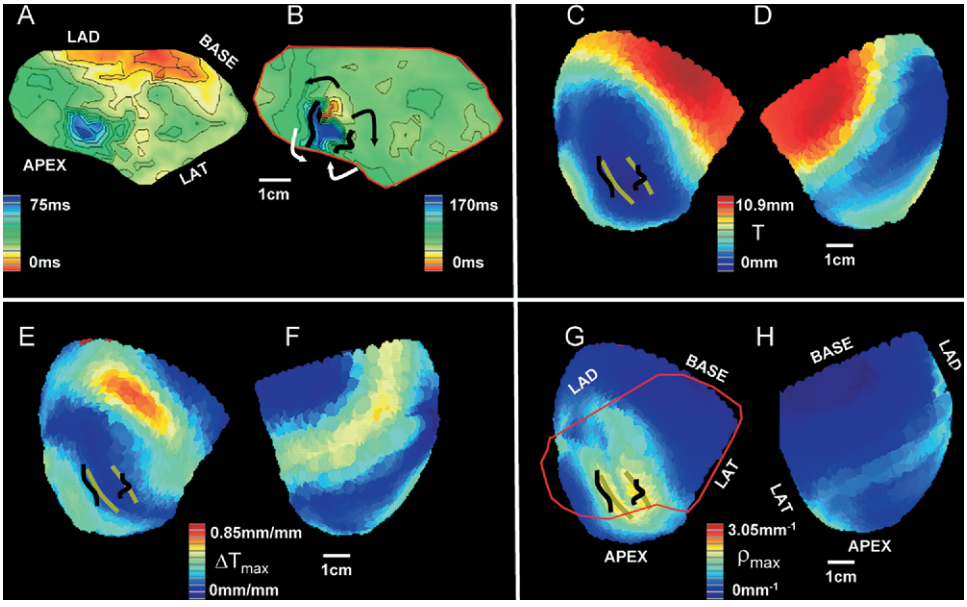

Figure 6 IBZ maps for postinfarction canine experiment in which only nonsustained reentrant tachycardia was inducible. Panels are the same as in Figure 5.

ρ_{max} is also proportional to $1/T$ (Equations 9 and 10). Thus, where thickness T is large (red and yellow in Figure 4C), ρ_{max} tends to be small (Figure 4E).

Activation mapping and analysis of infarct depth after MRI measurement is shown for an experiment with only inducible sustained reentrant ventricular tachycardia (Figure 5) and an experiment with only inducible nonsustained reentrant tachycardia (Figure 6). Sinus rhythm and ventricular tachycardia activation maps are given in Figures 5A, 5B, 6A, and 6B. The thickness map is given in panels C and D, maximum gradient in panels E and F, and maximum estimated curvature in panels G and H. On the curvature maps (panels G), multielectrode array position during electrogram recording is noted in red outline. Reentrant tachycardia is caused by a double-loop reentrant circuit in each experiment (Figures 5B and 6B) with relatively slow and late sinus

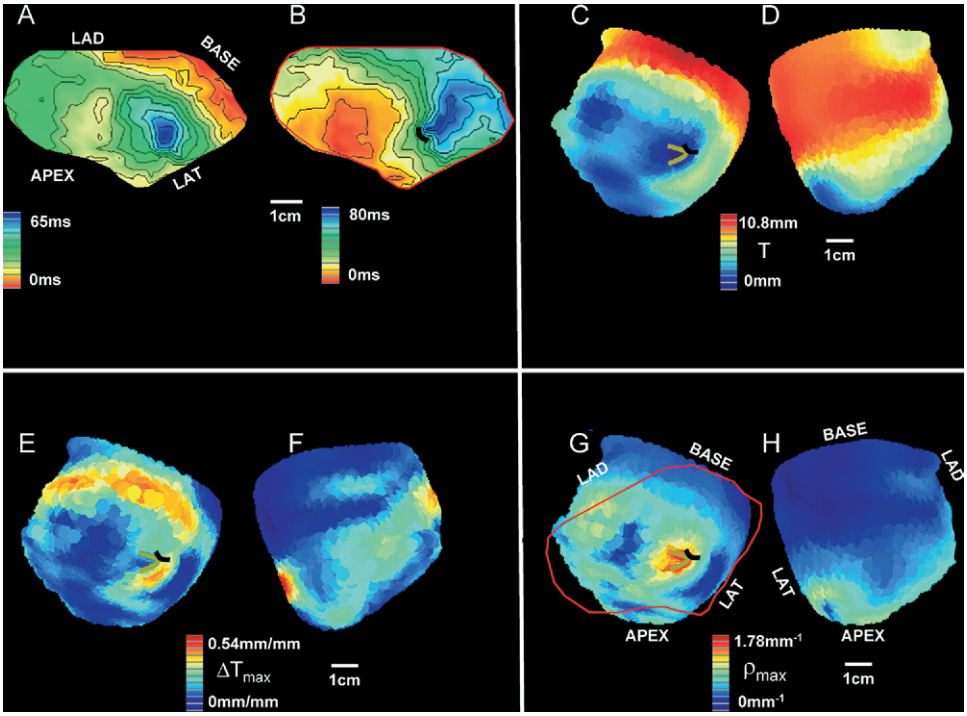

Figure 7 IBZ maps for postinfarction canine experiment in which a reentrant circuit was not mappable, although ventricular tachycardia was induced. Panels are the same as in Figure 5. Note isochronal spacing is ~5 ms in the sinus rhythm and ventricular tachycardia activation maps, panels **A** and **B**.

rhythm activation at the isthmus region (Figures 5A and 6A). The thinnest tissue occurs along a band oriented in the direction between the isthmus entrance and exit (Figures 5C and 6C). The largest ΔT_{max} occurs at the lateral edges of the thin tissue region where functional block lines form and also elsewhere along the edge of the IBZ (Figures 5E, 5F and 6E, 6F). The maximum degree of curvature ρ_{max} is coincident with the locations where IBZ thickness is minimal and the IBZ thickness spatial gradient is maximal, and actual block (black lines) approximately collocate with these points of maximum curvature (gray lines, Figures 5G and 6G, also shown overlapped in panels C and E). The predicted pathway is wider, and the degree of curvature at both the lateral edges and the ends of the isthmus location is less in the sustained versus the nonsustained experiment (Figures 5 and 6).

Activation mapping and analysis of infarct depth after MRI measurement are shown for an experiment with no mappable reentrant tachycardia (Figure 7). The panel labels correspond to those in Figures 5 and 6. The isochronal spacing in the activation maps of Figure 7A and 7B is 5 ms to show detail in the conduction pattern. The region of thinnest IBZ with large ρ_{max} at a border (Figure 7C, 7G) had slow and late sinus rhythm activation (Figure 7A). During tachycardia, which lacked a complete circuit on the mapping grid (Figure 7B), block occurred at the location of the maximum estimated wavefront curvature (Figure 7G). However, as predicted from Figure 7G, only a single short functional block line, rather than two parallel lines, was present during tachycardia (Figure 7B). Furthermore, the region of thinnest IBZ at the epicardial surface (Figure 7C) was small compared with corresponding regions in sustained and nonsustained reentry experiments (Figures 5C and 6C). MRI-generated reconstruction in this experiment (not shown) suggested that viable pathways of midmyocardial tissue may have provided a closed loop for reentry that would not be entirely mappable from the surface.

Summary statistics

During tachycardia, the reentry isthmus overlapped the thinnest IBZ region and was aligned with its long axis (Figures 4B, 4C, 5B, 5C, and 6B, 6C). In Figure 8, the overlap of estimated and actual block line location is shown for the six experiments with mappable double-loop reentry. The estimated ablation line (dashed) overlapped the actual isthmus width by a mean of 91.8% ± 4.6%. The mean distance between actual and estimated block line location was 6.5 ± 3.7 mm. The model equations were useful to detect the isthmus location with a sensitivity of 75.0% and a specificity of 97.2%.

Table 1 shows the statistical variables and can be summarized as follows. The mean thickness of the IBZ was much less within the isthmus location compared with outside the isthmus (231 ± 140 μm versus 1440 ± 770 μm; $P < .001$). The maximum degree of wavefront curvature (ρ_{max}) was 1.63 ± 0.45 mm^{-1}at block line locations, signifying that block would be expected to occur since the

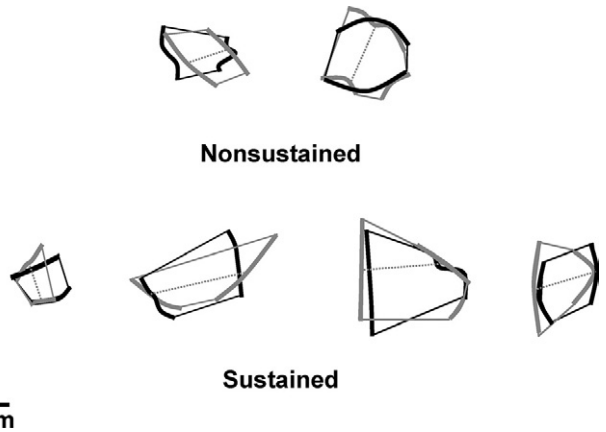

Figure 8 Overlap of estimated isthmus location (from maps derived using Equation 9) with actual isthmus location (from tachycardia activation map).

value was above 1.0. Mean ρ_{max} was less at entrance and exit points but still relatively high (0.71 ± 0.18 mm^{-1}), which suggests that conduction velocity would tend to slow at these locations. Mean ρ_{max} was least elsewhere in the circuit pathway (0.33 ± 0.13 mm^{-1}), which suggests that relatively rapid conduction velocity would occur in these areas. The means were significantly different ($P < .001$). The measured conduction velocities are in agreement with the calculations of ρ_{max}. The mean conduction velocity at entrance and exit points during tachycardia (0.32 ± 0.05 mm/ms) was slower than elsewhere in the circuit (0.42 ± 0.13 mm/ms). The areas of the circuit with minimal ΔT_{max} had significantly faster conduction velocity compared with the circuit as a whole (0.64 ± 0.16 mm/ms; $P < .001$). Compared with sustained tachycardia, in nonsustained tachycardia experiments there was greater ρ_{max} at block line locations and entrance and exit points and slower conduction velocity at entrance and exit points, and the IBZ was thicker outside the isthmus. The thicker mean IBZ away from the isthmus in nonsustained experiments likely resulted in a larger ΔT_{max} at the isthmus boundary, so that ρ_{max} at the boundary was increased compared with sustained experiments.

Discussion

In this study, a geometric formulation of the relationship between IBZ geometry and propagation of electrical activation wavefronts in reentrant circuits was developed. Based on the model, areas of slow conduction and block during reentry were expected to coincide with regions where IBZ thickness (T) was minimal and the thickness gradient (ΔT) was maximal, so that wavefront curvature ρ would be maximized. Also based on the model, regions of fastest conduction velocity were anticipated to coincide with areas of minimum ΔT. Model predictions were then compared with electrical and structural measurements in canine postinfarction. The implications of this study are now discussed.

Table 1 Geometry-propagation statistics

VT units	T_i, μm	T_o, μm	$\rho_{max,b}$, mm^{-1}	$\rho_{max,e}$, mm^{-1}	$\rho_{max,o}$, mm^{-1}	VT θ_e, mm/ms	VT θ_o, mm/ms	VT θ_f, mm/ms	Distance, mm
All (n = 6)	231 ± 140	1440 ± 770	1.63 ± 0.45	0.71 ± 0.18	0.33 ± 0.13	0.32 ± 0.04	0.42 ± 0.13	0.64 ± 0.16	6.45 ± 3.74
NSVT (n = 2)	226 ± 139	1753 ± 893	2.02 ± 0.42	0.85 ± 0.10	0.41 ± 0.15	0.25 ± 0.03	0.39 ± 0.09	0.60 ± 0.11	4.39 ± 1.81
MSVT (n = 4)	233 ± 144	1284 ± 671	1.37 ± 0.24	0.62 ± 0.16	0.27 ± 0.08	0.35 ± 0.05	0.44 ± 0.15	0.66 ± 0.18	7.48 ± 4.01

MSVT = monomorphic sustained tachycardia; NSVT = nonsustained tachycardia; VT = ventricular tachycardia; *i* = inner pathway; *o* = outer pathway; *f* = region with minimum ΔT_{max}; *b* = block lines; *e* = ends (entrance-exit sites).

Utility of the IBZ geometry model

For model calculations, IBZ thickness resolution was 0.4 mm in MRI images and ~1 μm in histology imaging studies. Although these methods had different resolution, both were found to be useful to distinguish areas where functional block would be expected to occur ($\rho > 1\ mm^{-1}$), as compared with slow conduction regions when present at the entrance and exit to the isthmus ($0\ mm^{-1} << \rho < 1\ mm^{-1}$) and rapid conduction regions elsewhere in the circuit ($\rho \sim 0\ mm^{-1}$). Thus, MRI of the heart,[3,9,10] which has high resolution and is noninvasive, was found to be useful to extract the geometric structure of the conducting medium for correlation with activation pattern characteristics. The geometric model that was described in this study is therefore also potentially useful to predict how the evolution of the structural properties of the tissue will affect reentry inducibility. For example, the period of arrhythmogenesis in canine postinfarction is not precisely known. However, regeneration of normal tissue with disappearance of the infarct and its BZ occurs over time. Presumably, the rate and character of structural changes will determine reentry inducibility as predicted by the model, but this must be tested. Cardiac MRI is also becoming a useful tool for analysis of postinfarction ventricular tachycardia in clinical patients. In human postinfarction, IBZ geometric properties are more permanent than in canine postinfarction, and arrhythmogenicity often continues so long as the patient remains untreated. The application of the IBZ geometry model for prediction of reentrant ventricular tachycardia and its characteristics in postinfarction patients is the subject of future research.

Other factors influencing wavefront propagation during reentry

Other studies have shown that although functional block lines are frequently aligned approximately in parallel with muscle fiber axis, off-axis and even transverse arcs of block bounding the reentry isthmus can occur.[23] We would expect anisotropy to increase the probability of longitudinal isthmus alignment because the higher resistance of ~1 kΩcm[24] that would be encountered laterally as the wavefront expands in the *XY* direction at an isthmus entrance or exit point would lessen the overall impedance mismatch and thereby increase the likelihood of propagation.[16–18] We would anticipate a decreased probability of transverse isthmus alignment due to the lowered resistance of ~500 Ωcm[24] encountered laterally at entrance-exit points, thus increasing the overall impedance mismatch and the likelihood of block.[16–18] For this reason, we would anticipate that transverse alignment would only be supported when the isthmus entrance and exit-points are wide with gradual thickness change so that three-dimensional convex wavefront curvature is reduced, the subject of future research.

At the isthmus region there is gap-junctional dissociation,[5,24,25] decreased sodium channel function,[15,24–26] and fewer viable myocytes,[4,11] all of which potentially result in greater cell-to-cell uncoupling with increased resistivity. If the increased resistivity due to these additional factors is inversely related to infarct distance as suggested previously by our group,[5] then at step increases in IBZ thickness outward from the isthmus, the sudden drop in resistivity would increase the likelihood of block because of the added load contribution (increased impedance mismatch). Thus these additional factors potentially act synergistically to reinforce the *Z*-axis curvature effect.

Estimate of contribution of other factors to functional block

In a previous canine postinfarction study, we measured a substantial change in longitudinal conduction velocity from the isthmus (θ_{IP} = 29 cm/s) to the outer circuit pathway (θ_{OP} = 37 cm/s) but negligible change in transverse conduction velocity from the isthmus (θ_{IP} = 19 cm/s) to the outer pathway (θ_{OP} = 17 cm/s).[24] Using the larger (longitudinal) difference and based on Equation 1 above, the maximum impedance mismatch from isthmus to outer pathway would be

$$R_i/R_o = \theta_o^2/\theta_i^2 = 1.63{:}1$$

We can estimate the impedance mismatch at which block will occur as follows. Suppose a circular wavefront has an initial radius $r = r_c$, the radius of critical curvature. Using r_c = 1 mm[17] and a space constant λ = 0.4 mm, the ratio of annular areas activating radially to one space constant from r_c in either direction is

$$[(r_c + \lambda)^2 - r_c^2]/[r_c^2 - (r_c - \lambda)^2] = (1.4^2 - 1)/(1^2 - .6^2) = 1.5.$$

Since the larger area radially outward from r_c would therefore require approximately 1.5*x* as much current for activation, a load of 1.5:1 or greater would be expected to cause block. Thus, almost all of the actual resistive change from isthmus to outer pathway, causing the maximal load of 1.63:1, would need to occur over a single space constant

(0.4 mm) for the wavefront to block. Thus one possible scenario in which functional block would occur would be a case in which almost all of the resistive change took place at the isthmus boundary. However, suppose as mentioned above that extracellular resistance is inversely proportional to infarct proximity. Using Figure 4C as an example, IBZ depth increases from ~100 μm within the isthmus to ~500 μm in the area immediately surrounding it (step transition of ~400 μm). Yet the mean depth of the outer pathway is 1284 μm for sustained reentry experiments (Table 1). Therefore, only ~1/3 of the total resistive change from inner to outer pathway would be expected to occur at the isthmus boundary (1 + 0.63/3 = 1.21:1), which would not be expected to independently cause functional block.

Muscle fiber branching is another factor that might be responsible for block in the IBZ during reentrant ventricular tachycardia. Previously, we measured an anisotropic ratio of ~2:1 in the IBZ (ratio of transverse to longitudinal resistance r_T/r_L ~ 4:1).[24] Therefore, were there to be a sudden change from transverse to longitudinal propagation in the direction of wavefront travel due to muscle fiber branching, functional block would likely occur. It would seem unlikely, however, that two such branching phenomena would be configured in such a way so as to generate approximately parallel block lines in proximity and cause the double-loop type of reentrant pattern that is common in both canine and human postinfarction ventricular tachycardia.

Previous studies have also suggested the important role of geometrical variations and structural discontinuities on wavefront propagation and on the constancy of reentrant circuit location during ventricular tachycardia.[16–18,22,27,28] The combined effect of all factors on reentrant ventricular tachycardia conduction: geometry, ionic and gap-junctional properties, and anisotropy can be determined using a heterogeneous ion-channel bidomain model.[25] However, because of the large number of state variables (degrees of freedom), it would be difficult to completely isolate the effect of each factor. To identify their relative contribution by ionic modeling, it would be useful to incorporate both high-resolution geometrical data as well as detailed molecular information measured at different depths and at different locations in the IBZ.

Limitations

In the geometric model, we did not account for the effect of partial-flux conditions[16] at the infarct boundary. The presence of partial-flux conditions increases wavefront curvature for any given angle β, thereby increasing the likelihood of block at the lateral isthmus boundary. At longer tachycardia cycle lengths (>200 ms), the critical radius of curvature r_c decreases,[17] thus decreasing the probability of functional block when ρ_{max} is in the range 1–4 mm^{-1} (Figures 4–7). Yet, as mentioned above, other factors likely contribute to the electrical load at the lateral isthmus boundary and help maintain functional block even at longer cycle lengths. The *XY* resolution of our multielectrode grid was ~4 mm × 4 mm. According to Nyquist's law, high-frequency spatial components of the traveling wave will be undersampled if the spatial resolution is insufficient, resulting in wavefront distortion. This is a potential source of error in conduction velocity calculation where wavefront curvature is high. We did not consider the possible role of myofibroblasts[29] and action potential duration[15,26] in governing the characteristics of reentrant ventricular tachycardia, which is a study limitation. Differences exist in canine versus human postinfarction reentrant ventricular tachycardias, including time to induction and myocardial location.[30] Yet, canine studies are potentially useful to determine the structural and molecular basis of ventricular tachycardia as well as for initiating clinical therapeutic strategies, including map-guided surgery, catheter ablation, and antitachycardia pacing.[30]

Acknowledgments

We thank Dr. Candido Cabo and Dr. Heather S. Duffy for helpful discussions, Dr. Truman Brown for use of his MRI laboratory, Dr. Elisa Konofagou for providing research materials, and Dr. Jaime G. Cruz-Lobo for technical assistance.

Appendix

Supplementary data

Supplementary data associated with this article can be found, in the online version, at doi:10.1016/j.hrthm.2007.04.015.

References

1. Wit AL. Ablation of ventricular tachycardia: does anyone have any new ideas? Heart Rhythm 2006;3:198–200.
2. Garan H. A perspective on the ESVEM trial and current knowledge: catheter ablation for ventricular tachyarrhythmias. Prog Cardiovasc Dis 1996;38:457–462.
3. Ashikaga H, Mickelsen SR, Ennis DB, Rodriguez I, Kellman P, Wen H, McVeigh ER. Electromechanical analysis of infarct border zone in chronic myocardial infarction. Am J Physiol Heart Circ Physiol 2005;289:H1099–H1105.
4. Wit AL, Allessie MA, Bonke FI, Lammers W, Smeets J, Fenoglio JJ Jr. Electrophysiologic mapping to determine the mechanism of experimental ventricular tachycardia initiated by premature impulses. Am J Cardiol 1982;49:166–185.
5. Peters NS, Coromilas J, Severs NJ, Wit AL. Disturbed connexin43 gap junction distribution correlates with the location of reentrant circuits in the epicardial border zone of healing canine infarcts that cause ventricular tachycardia. Circulation 1997;95:988–996.
6. Ciaccio EJ, Coromilas J, Costeas CA, Wit AL. Sinus rhythm electrogram shape measurements are predictive of the origins and characteristics of multiple reentrant ventricular tachycardia morphologies. J Cardiovasc Electrophysiol 2004;15:1293–1301.
7. Ciaccio EJ. Ventricular tachycardia duration and form are associated with electrical discontinuities bounding the core of the reentrant circuit. J Cardiovasc Electrophysiol 2005;16:646–654.
8. Costeas C, Peters NS, Waldecker B, Ciaccio EJ, Wit AL, Coromilas J. Mechanisms causing sustained ventricular tachycardia with multiple QRS morphologies: results of mapping studies in the infarcted canine heart. Circulation 1997;96:3721–3731.
9. Kim RJ, Fieno DS, Parrish TB, Harris K, Chen EL, Simonetti O, Bundy J, Finn JP, Klocke FJ, Judd RM. Relationship of MRI delayed contrast enhancement to irreversible injury, infarct age, and contractile function. Circulation 1999;100:1992–2002.
10. Faris OP, Evans FJ, Ennis DB, Helm PA, Taylor JL, Chesnick AS, Guttman MA, Ozturk C, McVeigh ER. Novel technique for cardiac electromechanical mapping with magnetic resonance imaging tagging and an epicardial electrode sock. Ann Biomed Eng 2003;31:430–440.
11. Dillon SM, Allessie MA, Ursell PC, Wit AL. Influences of anisotropic tissue

structure on reentrant circuits in the epicardial border zone of subacute canine infarcts. Circ Res 1988;63:182–206.
12. Ciaccio EJ, Chow AW, Davies AW, Wit AL, Peters NS. Localization of the isthmus in reentrant circuits by analysis of electrograms derived from clinical noncontact mapping during sinus rhythm and ventricular tachycardia. J Cardiovascular Electrophysiol 2004;15:27–36.
13. Ciaccio EJ, Tosti AC, Scheinman MM. Relationship between sinus rhythm activation and the reentrant ventricular tachycardia isthmus. Circulation 2001; 104:613–619.
14. MacLeod RS, Johnson CR. Map3d: Interactive scientific visualization for bioengineering data. IEEE Engineering Medicine Biology Society 15th Annual International Conference 1993:30–31.
15. Cabo C, Boyden P. Electrical remodeling of the epicardial border zone in the canine infarcted heart. Am J Physiol Heart Circ Physiol 2003;284:H372–H384.
16. Kogan BY, Karplus WJ, Billett BS, Stevenson WG. Excitation wave propagation within narrow pathways: geometric configurations facilitating unidirectional block and reentry. Physica D 1992;59:275–296.
17. Cabo C, Pertsov AM, Baxter WT, Davidenko JM, Gray RA, Jalife J. Wave-front curvature as a cause of slow conduction and block in isolated cardiac muscle. Circ Res 1994;75:1014–1028.
18. Kleber AG, Rudy Y. Basic mechanisms of cardiac impulse propagation and associated arrhythmias. Physiol Rev 2004;84:431–488.
19. Ramza BM, Tan RC, Osaka T, Joyner RW. Cellular mechanism of the functional refractory period in ventricular muscle. Circ Res 1990;66:147–162.
20. Clayton RH, Holden AV. Computational framework for simulating the mechanisms and ECG of re-entrant ventricular fibrillation. Physiol Meas 2002;23:707–726.
21. Sampson KJ, Henriquez CS. Interplay of ionic and structural heterogeneity on functional action potential duration gradients: implications for arrhythmogenesis. Chaos 2002;12:819–828.
22. Fast VG, Kléber AG. Role of wavefront curvature in propagation of cardiac impulse. Cardiovasc Res 1997;33:258–271.
23. Ciaccio EJ, Costeas C, Coromilas J, Wit AL. Static relationship of cycle length to reentrant circuit geometry. Circulation 2001;104:1946–1951.
24. Cabo C, Yao J, Boyden PA, Chen S, Hussain W, Duffy HS, Ciaccio EJ, Peters NS, Wit AL. Heterogeneous gap junction remodeling in reentrant circuits in the epicardial border zone of the healing canine infarct. Cardiovasc Res 2006;72:241–249.
25. Cabo C, Boyden PA. Heterogeneous gap junction remodeling stabilizes reentrant circuits in the epicardial border zone of the healing canine infarct: a computational study. Am J Physiol Heart Circ Physiol 2006;291:H2606–H2616.
26. Baba S, Dun W, Cabo C, Boyden PA. Remodeling in cells from different regions of the reentrant circuit during ventricular tachycardia. Circulation 2005;112: 2386–2396.
27. Spach MS, Heidlage JF, Barr RC, Dolber PC. Cell size and communication: role in structural and electrical development and remodeling of the heart. Heart Rhythm 2004;1:500–515.
28. Pertsov AM, Davidenko JM, Salomonsz R, Baxter WT, Jalife J. Spiral waves of excitation underlie reentrant activity in isolated cardiac muscle. Circ Res 1993; 72:631–650.
29. Miragoli M, Gaudesius G, Rohr S. Electrotonic modulation of cardiac impulse conduction by myofibroblasts. Circ Res 2006;98:801–810.
30. Janse MJ, Opthof T, Kleber AG. Animal models of cardiac arrhythmias. Cardiovasc Res 1998;39:165–177.